

Turbulence modulation by dense suspensions in channel flows.

Francesco Picano

Department of Industrial Engineering
University of Padova
Via Venezia 1, 35131, Padova, Italy
francesco.picano@unipd.it

Pedro Costa

Laboratory for Aero and Hydrodynamics,
Delft University of Technology,
Leeghwaterstraat 21, NL-2628 CA Delft, The Netherlands
p.simoescosta@tudelft.nl

Wim-Paul Breugem

Laboratory for Aero and Hydrodynamics,
Delft University of Technology,
Leeghwaterstraat 21, NL-2628 CA Delft, The Netherlands
W.P.Breugem@tudelft.nl

Luca Brandt

SeRC (Swedish e-Science Research Centre) and Linné FLOW Centre,
KTH Mechanics,
SE-100 44 Stockholm, Sweden
luca@mech.kth.se

ABSTRACT

Dense suspensions are usually investigated in the laminar limit where inertial effects are insignificant. In this regime, the main effect of the suspended phase is to alter the rheological behavior of the flow which always displays higher effective viscosity with respect to the carrier fluid. When the flow rate is high enough, i.e. at high Reynolds number, the flow may become turbulent and the interaction between solid and liquid phase modifies the turbulent dynamics that we know in single-phase fluids. In the present work, we study turbulent channel flows laden with finite-size particles at high volume fraction ($\Phi = 0.2$) by means of Direct Numerical Simulations. A direct-forcing Immersed Boundary Method has been adopted to couple liquid and solid phases. The two-phase simulations have been performed fixing the bulk Reynolds number at $Re_b = U_b 2h/\nu = 12000$ (U_b bulk velocity, h channel half-width and ν the fluid kinematic viscosity). The particle size is relatively large with respect to the viscous length, i.e. 10 and 20 times, but smaller than large scales. We will present a detailed comparison of the statistical behavior of the particle-laden flow and the corresponding single-phase flow. The presence of the solid phase strongly alters the wall turbulence dynamics and its effect cannot be accounted only considering the higher rheological effective viscosity.

INTRODUCTION

Turbulent particle suspensions are frequently found in environmental and industrial flows such as mood and planetary flows, fluidized bed and hopper dredger. These flows are often so dense that the mutual particle-fluid interactions determine the overall dynamics. In most cases the suspended particles are also large with respect to the smallest scales present in the flow and directly interact with the macroscopic flow dynamics, so-called finite-size particles.

As regards dense suspension of solid particles, most of the previous studies are conducted in the presence of negligible inertia and small particles focusing on the rheological aspects of the flow. In

the seminal work of Einstein (1906), the effective viscosity of a suspension of rigid spheres is analytically derived for the dilute viscous limit: $\nu_e = \nu(1 + (5/2)\Phi)$, where ν is the kinematic viscosity of the suspending fluid, and Φ the bulk solid volume fraction. Several studies considered denser cases and different semi-empirical formula have been proposed to calculate the effective suspension viscosity, e.g. Eilers formula $\nu_e = \nu(1 + 5/4(\Phi/(1 - \Phi/\Phi_{max})))^2$ with Φ_{max} the maximum packing fraction Stickel & Powell (2005); Guazzelli & Morris (2011) for reviews.

Nonetheless in practical cases, the Reynolds number, which measures the importance of inertial on viscous effects, is usually high that the flow is turbulent. While turbulent wall-bounded flows have been thoroughly studied either in single-phase or dilute multi-phase conditions (Ferrante & Elghobashi, 2003; Soldati & Marchioli, 2009; Balachandar & Eaton, 2010), much less is known on their behaviors with a dense solid phase (Prosperetti, 2015). Shao *et al.* (2012) report results for turbulent channel flow up to 7% volume fraction showing a decrease of the fluid streamwise velocity fluctuation due to an attenuation of the large-scale streamwise vortices. Lashgari *et al.* (2014, 2016) show how different is the transition dynamics from the laminar to turbulent regime when a dense suspension is considered. They illustrate that for these complex flows three different regimes exist in the space $\Phi - Re$ with smooth transition among them. Each regime is characterized by the origin of the most relevant stress, viscous for the laminar, Reynolds for the turbulent and particle-stress for the dense (shear-thickening) regime. A first description of a dense suspension of finite-size particles in a turbulent channel flow is presented in Picano *et al.* (2015). In this work relatively low Reynolds number cases have been considered ($Re_b = 5600$), but with volume fraction up to $\Phi = 20\%$. They observed an increase of the overall drag increasing volume fraction originated by the presence of the particle stress absent in single-phase turbulent flows. Actually, they also noted a decrease of the turbulent activity at high volume fraction. However, given the rela-

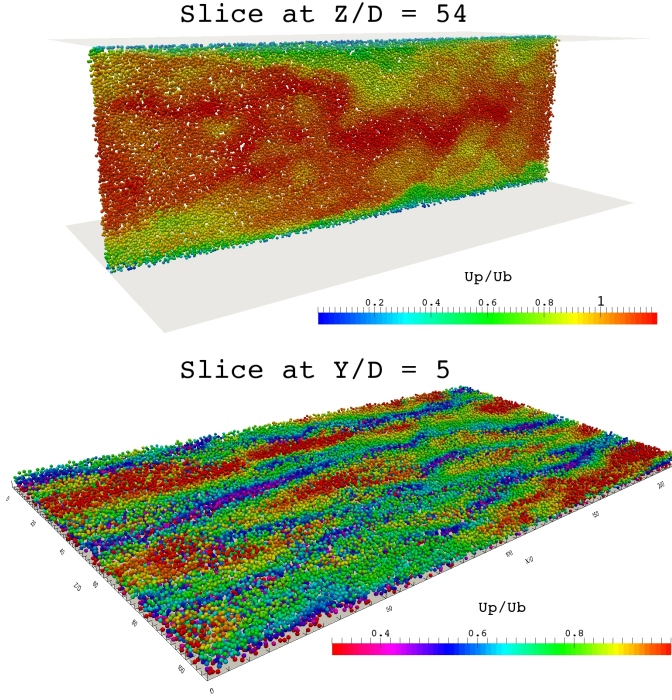


Figure 1. Snapshot of the particle position for the D10 cases. Only the particles in a narrow slice aligned with the streamwise-wallnormal plane (top-panel) and with the streamwise-spanswise plane (bottom-panel) are represented. Colors denote particle streamwise velocity normalized by the bulk velocity.

tively low Reynolds number it is difficult to draw general conclusion on the behavior of suspension in a fully developed turbulent regime. This aspect constitutes the main aim of the present work.

We consider here a pressure-driven turbulent plane-channel flow characterized by a fixed bulk Reynolds number $Re_b = U_b 2h/\nu = 12000$ with U_b the bulk velocity, h the channel half-width and ν the fluid kinematic viscosity. We performed interface-resolved Direct Numerical Simulations (DNS) of particle-laden channel flows at moderate Reynolds number with two different particle sizes and we compared the results with corresponding single-phase flows.

METHODOLOGY

We numerically solve the Navier-Stokes equations of an incompressible Newtonian fluid in a plane channel,

$$\rho \left(\frac{\partial \mathbf{u}}{\partial t} + \mathbf{u} \cdot \nabla \mathbf{u} \right) = -\nabla P + \mu \nabla^2 \mathbf{u} + \rho \mathbf{f}, \quad (1)$$

$$\nabla \cdot \mathbf{u} = 0,$$

where ρ is the density of both fluid and particles implying the neutrally buoyant particles and μ and P are the fluid viscosity and pressure respectively. The presence of finite size particles is treated by introducing local force at the vicinity of each particle surface, \mathbf{f} , added on the right hand side of the Navier-Stokes equation as usual in the Immersed Boundary Method. A second order finite-difference scheme on a staggered mesh is adopted for the spatial discretization. The time integration is performed by a third order Runge-Kutta method. Periodic boundary conditions (BC) are assigned in the streamwise (x) and spanwise (z) directions at distances

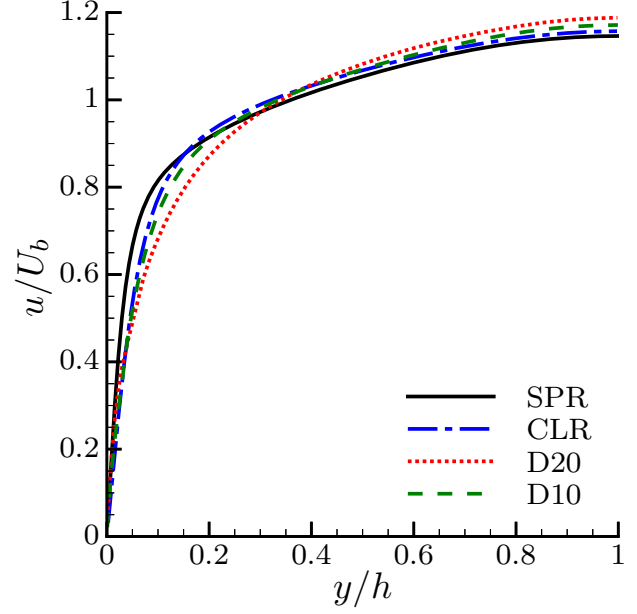


Figure 2. Mean fluid velocity normalized by the bulk velocity, u/U_b as a function of the wall normal distance y/h .

of $6h$ and $3h$ respectively, and no-slip/no-penetration (ns/np) at the bottom ($y = 0$) and top ($y = 2h$) walls. The motion of the spherical particles is governed by Newton-Euler equations

$$m^p \frac{d\mathbf{U}_c^p}{dt} = \oint_{\partial V_p} [-PI + \mu(\nabla \mathbf{u} + \nabla \mathbf{u}^T)] \cdot \mathbf{n} dS + \mathbf{F}_c, \quad (2)$$

$$I^p \frac{d\boldsymbol{\Omega}_c^p}{dt} = \oint_{\partial V_p} \mathbf{r} \times \{ [-PI + \mu(\nabla \mathbf{u} + \nabla \mathbf{u}^T)] \cdot \mathbf{n} \} dS + \mathbf{T}_c,$$

where m^p and I^p , \mathbf{U}_c^p and $\boldsymbol{\Omega}_c^p$ are the mass, moment inertia, center velocity and rotation rate of particle p . The surface of the particles and unit normal vector are denoted by ∂V_p and \mathbf{n} whereas the vector connecting the center to the surface of the particles is denoted by \mathbf{r} . The first term in right hand sides of these equations represents the net force/moment on particle p resulting from hydrodynamic interactions. The force and torque resulting from contact interactions are indicated by \mathbf{F}_c and \mathbf{T}_c . In these terms, lubrication corrections for sub-grid particle-particle and particle-wall interactions are used together with a soft-sphere collision model for solid-solid contacts, see Lambert *et al.* (2013) for additional details. The interface condition is introduced to enforce the fluid velocity at each point of the particle surface to be equal to the particle velocity at that point, $\mathbf{u}(\mathbf{X}) = \mathbf{U}^p(\mathbf{X}) = \mathbf{U}_c^p + \boldsymbol{\Omega}_c^p \times \mathbf{r}$. An Immersed Boundary Method with direct forcing developed by Uhlmann Uhlmann (2005) and modified by Breugem Breugem (2012) is employed to satisfy the interface condition by applying the forcing \mathbf{f} in the vicinity of each particle surface. The method has been tested and validated against several benchmark tests Costa *et al.* (2015); Picano *et al.* (2015); Lashgari *et al.* (2016). The present simulations impose a constant mass flux that fixes the bulk Reynolds number to $Re_b = 12000$. Two different particle sizes of $D_p/(2h) = 1/72$ (D10) and $1/36$ (D20) are simulated, corresponding to about 10 and 20 viscous lengths of a corresponding single-phase simulation. The bulk volume fraction is fixed to $\Phi = 20\%$. These simulations are complemented with a single-phase reference case (SPR) with the same Re_b number and a 'continuum-limit' reference (CLR) where single-phase flow is simulated with $Re_b = 6400$ to match the bulk Reynolds number based

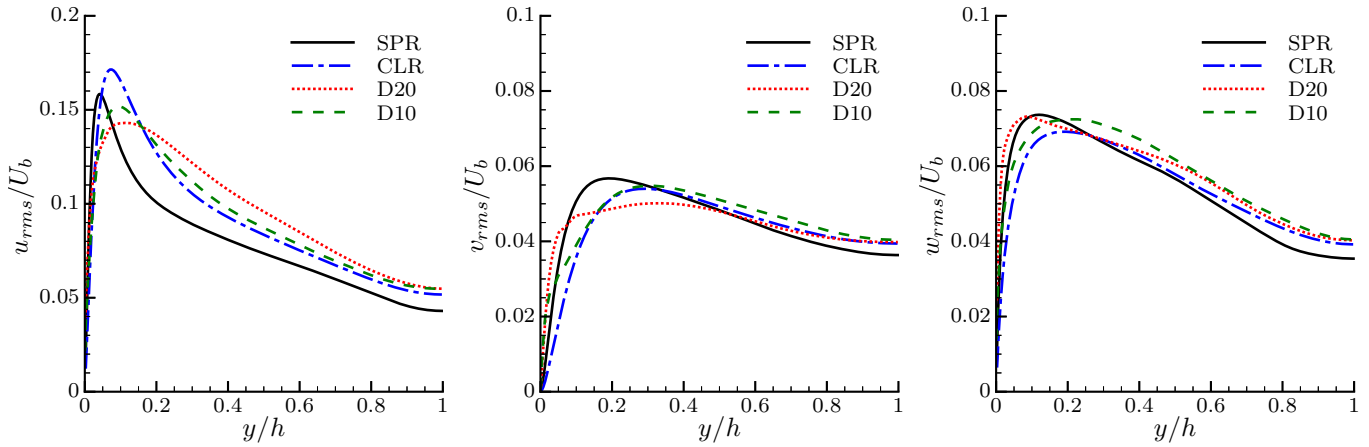


Figure 3. Root-Mean-Square of the fluid velocity fluctuations normalized by the bulk velocity as a function of the wall normal distance y/h . From left to right panel: streamwise component u_{rms}/U_b , wallnormal component v_{rms}/U_b , spanwise component w_{rms}/U_b

on the effective suspension viscosity at $\Phi = 20\%$, i.e. $U_b 2h/\nu_e$; see also table 1 for a summary of the parameters. A cubic mesh is adopted with size $\Delta = D_p/16$ and each particle surface contains 746 Lagrangian control points. For the smaller particles (D10), the mesh counts $3456 \times 1152 \times 1728$ points in the streamwise, wallnormal and spanwise directions, respectively. The number of particles adopted in the simulations are fixed at 640000 and 80000 for the D10 and D20 cases, respectively. An exemplum of the flow field laden with the smaller particles (D10) is provided in Figure 1.

RESULTS AND DISCUSSION

The presence of the solid phase alters the turbulence behavior in the channel flow with respect to the single-phase flow. In particular, we first extract the friction Reynolds number of the performed two-phase simulations, see table 1. The friction Reynolds number based on the fluid viscosity, $Re_\tau = u_\tau h/\nu$ ($u_\tau = \sqrt{\tau_w/\rho}$ the friction velocity and τ_w the wall stress), is always much higher than the single-phase flow case performed at the same fixed bulk Reynolds number based on the fluid viscosity (SPR). Hence the presence of particles in these conditions always increases the overall drag. In order to account the rheological features of a dense suspension we can calculate the friction Reynolds number based on the effective suspension viscosity ν_e , $Re_\tau^e = u_\tau h/\nu_e$, and compare with the corresponding single-phase flow which shares the bulk Reynolds number based on the effective viscosity ν_e (CLR). As it can be seen from table 1, the effective viscosity friction Reynolds number is higher than that obtained for the corresponding single phase flow (CLR) and the difference increases with the particle size. It means that the presence of finite-size particles in a turbulent flow cannot be accounted only considering the increased effective viscosity of the suspension.

The mean fluid velocity u/U_b with respect to the wall normal distance y/h , figure 2, shows significant differences with respect to the SPR case which consists on a single-phase flow with the same bulk Reynolds number. The largest difference appear in the near-wall region where the profile of the particle-laden cases strongly differ from the corresponding single-phase flows. The case at the corresponding effective Reynolds number (CLR), which accounts for the higher effective viscosity of the suspension, appears more similar, even though important differences still are present in the near wall region. This aspect suggests that the effective viscosity only is not sufficient to describe turbulent suspensions, although the predictions are significantly improved. In particular, the simulation with smaller particles (D10) is better approximated by the single-

phase flow with the same effective viscosity (CLR). Hence, the difference found between our particle-laden flows and the single-phase one which accounts for the suspension rheology can be ascribed to a particle finite-size effect. In case of very small particles the direct interaction between the particle dynamics and the flow features is not important because of the wide scale separation and the rheological features should be sufficient to determine the flow dynamics. Conversely with particles larger than the viscous length scale a different flow dynamics is observed especially in the near wall region.

In figure 3 the root-mean-square (rms) of the fluid velocity fluctuations of the streamwise u_{rms} , wallnormal v_{rms} and spanwise w_{rms} components vs y/h are shown for the two-phase and single-phase flows. The presence of the solid phase strongly alters the behavior of the wall turbulence especially in the near-wall region. In particular, we note that the peaks of fluid velocity fluctuations are always reduced by the particle presence. Larger the particles stronger the reduction. In addition, we note an enhancement of fluid fluctuation intensities close to the wall. We attribute this effect to the particle collisions/rebounds at the wall, that stir the fluid in this region, and to the large slip velocity of the particles which forces the fluid to move around the particles themselves. We remark that both the corresponding single-phase cases (SPR and CLR) fail to represent the fluctuating behavior of the two-phase flow. This indicates once again that finite-size effects are crucial for the turbulent dynamics even with particle sizes of about ten viscous lengths.

A better understanding of the effects of finite-size particles on

Table 1. Characterization of the present simulations. Volume fraction Φ ratio between particle diameter and channel half-width $D_p/(2h)$. Different definition of the Reynolds numbers: bulk Re number $Re_b = U_b 2h/\nu$; friction Re number $Re_\tau = u_\tau h/\nu$ (u_τ friction velocity); effective friction Re number $Re_\tau^e = u_\tau h/\nu_e$ with $\nu_e(\Phi)$ the rheological effective suspension viscosity

	Φ	$D_p/(2h)$	Re_b	Re_τ	Re_τ^e
D10	0.2	1/72	12000	395	209
D20	0.2	1/36	12000	406	215
SPR	0.0	*	12000	350	350
CLR	0.0	*	6400	201	201

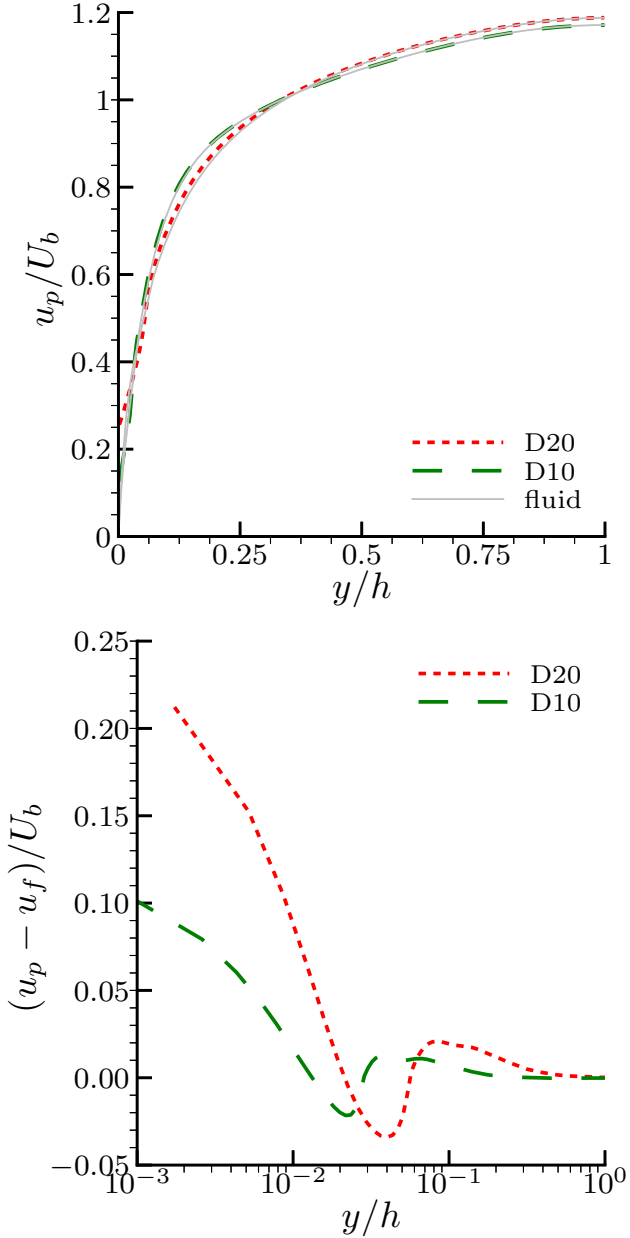


Figure 4. Top panel: mean particle velocity normalized by the bulk velocity, u_p/U_b as a function of the wall normal distance y/h . Bottom panel: difference between the mean particle and fluid velocity $(u_p - u_f)/U_b$ as a function of the wall normal distance y/h in log scale.

turbulent channel flow can be obtained looking at the particle velocity statistics. In the top panel of figure 4 the mean particle velocity u_p/U_b is shown with respect to the wall normal distance y/h . As it can be seen, small differences are present in the bulk of the flow. A more attentive observation in the near wall region shows significant differences between the particle and fluid mean velocity. In particular, since the particle velocity does not fulfill the no-slip condition as the fluid, particles show a not vanishing velocity at the wall. Defining the mean slip velocity as the difference between particle and fluid mean velocity $(u_p - u_f)/U_b$ at same location allows to quantify how intense is this effect through the channel. The bottom panel of figure 5 show the mean slip velocity with respect to the wall-normal distance y/h displayed in log-scale. The mean slip

is small in the bulk of the flow $y/h > 0.1$, while is significant and positive close to the wall. Larger the particles higher the slip. In the D10 case we note a slip of the order of 10% of the bulk velocity while it almost doubles for the D20 cases showing a nearly linear behavior with the particle size. The presence of this layer of particles which moves faster than the fluid changes the dynamics of the turbulence in the near wall region and is a cause of the increase of the overall drag caused by the particles, see Costa *et al.* (2016, 2017) for a detailed discussion of this effect. Interestingly, we note also a negative minimum around one particle diameter for the slip velocity. We attribute this effect to the first layer of particles which forms close to the wall because of the geometrical constrain induced by the planar solid wall. The midpoint in the wall-normal direction of this particle layer travels faster than the corresponding fluid, but the fluid at the edge of this layer towards the bulk is free to move faster than the solid particle layer.

Figure 5 shows the particle velocity rms of the streamwise $u_{p,rms}/U_b$, wallnormal $v_{p,rms}/U_b$ and spanwise $w_{p,rms}/U_b$ components with respect to the wall-normal distance y/h . The fluctuating behavior of the solid phase in the bulk of the channel is similar to that of the corresponding fluid phase. In this region, only the D20 case shows fluctuation levels lower than the fluid. Differences are observed in the near wall region (buffer layer) where the peak values shown by the solid phase are smaller than those of the fluid. An exception is found in the region adjacent to the wall. In this narrow region, we always find fluctuation levels higher for the solid phase than the fluid. It should be remarked that since particles do not comply with the no-slip condition, but respect only with the no-penetration condition, the rms of the streamwise and spanwise velocities are not vanishing at the wall. The wallnormal component is instead null, but suddenly increases departing from the wall. Actually, particles coming from the bulk can collide/rebound at the wall transporting and exchanging a significant amount of momentum. This effect explains the high levels of particle velocity fluctuations shown in this region that in turns excite the flow velocity fluctuations stirring the fluid between particles and wall during the collision. This dynamics justifies the increase of particle and fluid velocity fluctuations close to the wall with respect to the corresponding single-phase flow. It should be noted that this effect has to be ascribed to a direct interaction between the finite-size particle and the flow so it cannot be accounted only using rheological suspension features such as the effective viscosity.

FINAL REMARKS

The present particle-resolved direct numerical simulations show how important can be the finite-size effect in dense particle-laden turbulent channel flows. We always note an increase of the overall drag for the analyzed cases induced by the presence of the dense solid phase. Taking into account only for the effective viscosity of the suspension, though improve the flow prediction, is not sufficient to determine the actual turbulent flow behavior. In particular, we have shown how different is the solid phase dynamics from the fluid one in the near wall region. Particles do not comply with the no-slip wall boundary condition and this phenomenon strongly influences the observed different dynamical behavior close to the wall. In this region, the solid phase shows a positive mean slip with respect to the fluid. In the region adjacent to the wall, particles show higher velocity fluctuations. On the contrary, they attenuate the flow fluctuations in the buffer layer region reducing the turbulent velocity rms peaks. The bulk of the flow is instead less altered by the presence of the solid phase. We retain that the near-wall turbulence modulation operated by the particles is responsible for the overall drag increase.

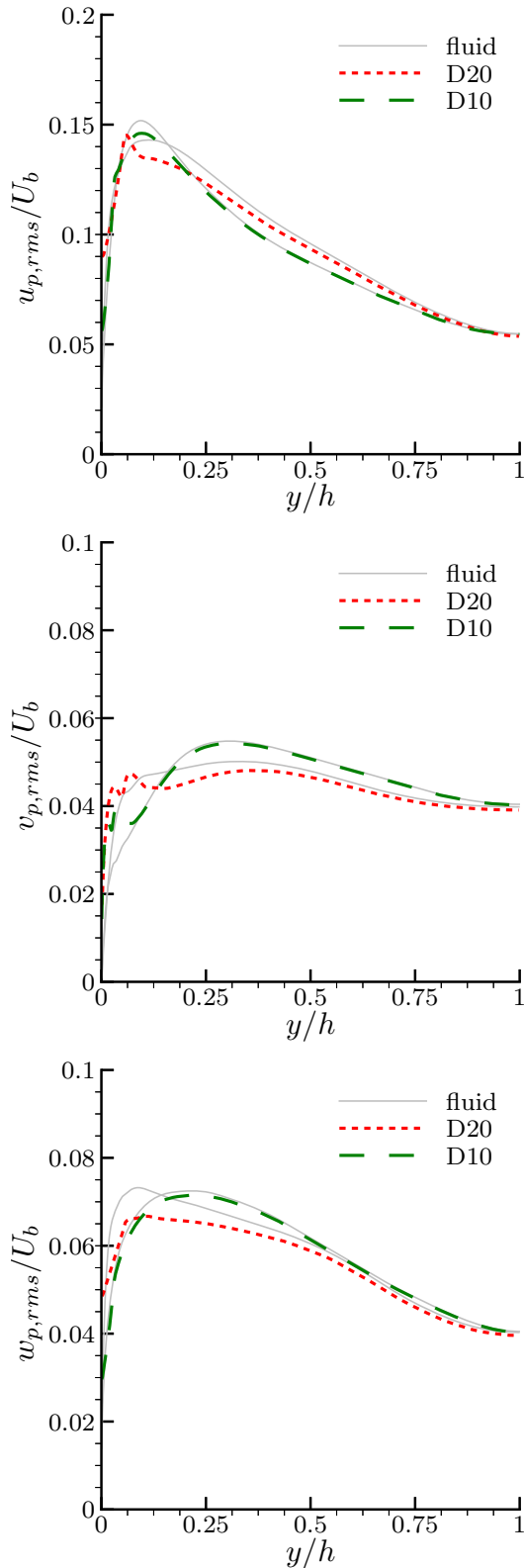


Figure 5. Root-Mean-Square of the particle velocity fluctuations normalized by the bulk velocity as a function of the wall normal distance y/h . From top to bottom panel: streamwise component $u_{p,rms}/U_b$, wallnormal component $v_{p,rms}/U_b$, spanwise component $w_{p,rms}/U_b$

Acknowledgements

This work was supported by the Portuguese Foundation for Science and Technology under Grant No. SFRH/BD/ 85501/2012, by the European Research Council Grant No. ERC-2013-CoG-616186, TRITOS, by the Swedish Research Council (V. R.) and by COST Action MP1305: Flowing Matter. We acknowledge computer time provided by SNIC (Swedish National Infrastructure for Computing), CINECA (ISCR Grant No. FIShNET-HP10CQQF77) and PRACE Project No. 2014112543 for awarding us access to resource CURIE based in France at Genci/CEA.

REFERENCES

- Balachandar, S & Eaton, John K 2010 Turbulent dispersed multiphase flow. *Annu. Rev. Fluid Mech.* **42**, 111–133.
- Breugem, Wim-Paul 2012 A second-order accurate immersed boundary method for fully resolved simulations of particle-laden flows. *Journal of Computational Physics* **231** (13), 4469 – 4498.
- Costa, Pedro, Boersma, Bendiks Jan, Westerweel, Jerry & Breugem, Wim-Paul 2015 Collision model for fully resolved simulations of flows laden with finite-size particles. *Physical Review E* **92** (5), 053012.
- Costa, Pedro, Picano, Francesco, Brandt, Luca & Breugem, Wim-Paul 2016 Universal scaling laws for dense particle suspensions in turbulent wall-bounded flows. *Physical Review Letters* **117** (13), 134501.
- Costa, Pedro, Picano, Francesco, Brandt, Luca & Breugem, Wim-Paul 2017 Finite size effects in dense turbulent wall-bounded transport of neutrally-buoyant spheres. *arXiv preprint arXiv:1703.06036*.
- Einstein, Albert 1906 On the theory of the brownian movement. *Annalen der physik* **4** (19), 371–381.
- Ferrante, A & Elghobashi, S 2003 On the physical mechanisms of two-way coupling in particle-laden isotropic turbulence. *Phys. Fluids* **15** (2), 315–329.
- Guazzelli, Elisabeth & Morris, Jeffrey F 2011 *A physical introduction to suspension dynamics*, vol. 45. Cambridge University Press.
- Lambert, Ruth A., Picano, Francesco, Breugem, Wim-Paul & Brandt, Luca 2013 Active suspensions in thin films: nutrient uptake and swimmer motion. *Journal of Fluid Mechanics* **733**, 528–557.
- Lashgari, Iman, Picano, Francesco, Breugem, Wim-Paul & Brandt, Luca 2014 Laminar, turbulent, and inertial shear-thickening regimes in channel flow of neutrally buoyant particle suspensions. *Phys. Rev. Lett.* **113**, 254502.
- Lashgari, Iman, Picano, Francesco, Breugem, Wim Paul & Brandt, Luca 2016 Channel flow of rigid sphere suspensions: Particle dynamics in the inertial regime. *International Journal of Multiphase Flow* **78**, 12 – 24.
- Picano, Francesco, Breugem, Wim-Paul & Brandt, Luca 2015 Turbulent channel flow of dense suspensions of neutrally buoyant spheres. *Journal of Fluid Mechanics* **764**, 463–487.
- Prosperetti, Andrea 2015 Life and death by boundary conditions. *Journal of fluid mechanics* **768**, 1–4.
- Shao, Xueming, Wu, Tenghu & Yu, Zhaosheng 2012 Fully resolved numerical simulation of particle-laden turbulent flow in a horizontal channel at a low reynolds number. *Journal of Fluid Mechanics* **693**, 319–344.
- Soldati, A. & Marchioli, C. 2009 Physics and modelling of turbulent particle deposition and entrainment: Review of a systematic study. *International Journal of Multiphase Flow* **35** (9), 827–839.
- Stickel, Jonathan J. & Powell, Robert L. 2005 Fluid mechanics and rheology of dense suspensions. *Annual Review of Fluid Mechanics* **37** (1), 129–149.

Uhlmann, M. 2005 An immersed boundary method with direct forcing for simulation of particulate flow. *J. Comput. Phys.* **209**, 448–

476 .